



**Frac Sand Crushing Characteristics and Morphology Changes  
under High Compressive Stress and Implications for Sand  
Pack Permeability**

Journal:	<i>Canadian Geotechnical Journal</i>
Manuscript ID	cgj-2016-0045.R1
Manuscript Type:	Article
Date Submitted by the Author:	27-Apr-2016
Complete List of Authors:	Zheng, Wenbo; University of British Columbia, School of Engineering Tannant, Dwayne; University of British Columbia, School of Engineering
Keyword:	Frac sand; sand crushing; grain shape; sand pack permeability



# Frac Sand Crushing Characteristics and Morphology Changes under High Compressive Stress and Implications for Sand Pack Permeability

Wenbo Zheng and Dwayne Tannant

Wenbo Zheng. School of Engineering, University of British Columbia, Kelowna, BC V1V 1V7,  
Canada. (e-mail: [wbzheng@alumni.ubc.ca](mailto:wbzheng@alumni.ubc.ca))

Dwayne Tannant. School of Engineering, University of British Columbia, Kelowna, BC V1V  
1V7, Canada. (e-mail: [dwayne.tannant@ubc.ca](mailto:dwayne.tannant@ubc.ca))

\*Corresponding author: Wenbo Zheng. School of Engineering, University of British Columbia,  
Kelowna, BC V1V 1V7, Canada. Phone number: 1.250.899.5902. E-mail:  
[wbzheng@alumni.ubc.ca](mailto:wbzheng@alumni.ubc.ca)

1           **ABSTRACT:** Sand consisting of round quartz grains is widely used as a proppant during  
2 hydraulic fracturing to produce natural gas from tight shale formations. This paper presents  
3 results from sand characterization and crushing tests on Jordan Formation frac sand. It includes  
4 an assessment of grain size reduction, changes in particle shape, and reduction in void ratio. It  
5 also examines the implications for permeability reduction through a sand pack caused by the  
6 closure stress on a hydraulic fracture. The sand from two size ranges (0.6 to 0.71 mm and 0.5 to  
7 0.6 mm) was tested dry under applied compressive stresses of up to 40 MPa in a crushing cup.  
8 The overall sand pack stress-strain response becomes softer as grains are crushed. The particle  
9 shape shifts from nearly spherical grains to diametrically split grains and then to small elongated  
10 and angular fragments for the smaller particle sizes. The permeability of the sand pack reduces  
11 by more than 40% at a 20 MPa stress, which is mainly caused by a decrease in void ratio due to  
12 compaction. The permeability reduces by over 70% at a 40 MPa stress, which is primarily  
13 caused by void ratio decrease, reduction in particle size, and a shift away from spherical particle  
14 shapes. Compared to the ISO 13503-2 standard where only the sand crushing percentage after  
15 crushing tests is measured, this paper demonstrates that more information can be extracted from  
16 sand crushing tests and that sand pack permeability can be assessed to optimize frac sand  
17 selection. A sand with a larger size range has a higher crushing percentage but is more permeable  
18 compared to a sand with a smaller size range. This further indicates that frac sand selection based  
19 only on sand crushing percentage is not sufficient to achieve a better sand pack permeability.

20 **Keywords:** Frac sand; sand crushing; grain shape; sand pack permeability

21

22

## 23 Introduction

24 Frac sand is widely used as a proppant for hydraulic fractures used to increase the  
25 recovery rate of hydrocarbons in oil and gas industry. The North American market consumes  
26 more than 80% of the world's supply of frac sand and nearly 50% of this frac sand is mined in  
27 Wisconsin (Benson and Wilson 2015). Typically hydraulic fractures in tight shale formations are  
28 created several kilometres beneath the ground surface. Fracturing fluids transport proppants to  
29 newly-created fractures and a proppant pack is then formed within the fractures. After hydraulic  
30 fracturing, stress from the surrounding formations will act on the hydraulic fractures. This stress  
31 is called the closure stress and it tends to reduce the aperture of fractures. A proppant pack is  
32 designed to resist the closure stress and prop open fractures, and act as paths for oil and gas to  
33 flow. The closure stress for different shale formations varies but is typically larger than 30 MPa,  
34 e.g. 60 MPa to 80 MPa for Haynesville Shale, less than 40 MPa for Fayetteville Shale, and  
35 roughly 40 MPa for the Montney Shale (Song and Hareland 2012). The high closure stress acting  
36 on proppants within the hydraulic fractures often crushes proppant grains into smaller fragments  
37 (Palisch et al. 2009). For example, crushed sand was observed in flow back tests from the  
38 Montney Formation under a closure stress of 42.3 MPa (Romanson et al. 2010). Proppant  
39 crushing allows the hydraulic fracture to close thus reducing the fracture aperture. Furthermore,  
40 the presence of small fragments of crushed sand decreases the permeability or hydraulic  
41 conductivity of the proppant pack because they can block natural gas flow paths. Coulter et al.  
42 (1972) and Lacy et al. (1997) both found that 5% fines can cause an over 50% reduction in the  
43 proppant pack conductivity, which is defined as the proppant pack permeability times the  
44 fracture aperture. A study for the Bakken Formation showed that the permeability of a ceramic  
45 proppant pack was five times higher than that of Ottawa sand under approximately 50 MPa

46 closure stress. The higher permeability was attributed to the higher crushing resistance of the  
47 ceramic proppants (Kurz et al. 2013).

48 Sand crushing was noted by Terzaghi and Peck (1948) in one-dimensional compression  
49 tests on sands subjected to 95.6 MPa. Many studies have quantified a change in the grain size  
50 distribution due to crushing (Lade et al. 1996; Zhang and Baudet 2013) and its effect on  
51 macroscopic properties of the sand, e.g., density, void ratio, friction angle, critical state line, etc.  
52 (Chuhan et al. 2002; Luzzani and Coop 2002; Coop 2004; Ghafghazi et al. 2014). A single-  
53 particle crushing test was used to measure the crushing characteristics and strength statistics of  
54 quartz, orthoclase, and plagioclase sand grains (Nakata et al. 1999). Parab et al. (2014) used x-  
55 ray computed tomography to observe sand crushing under static loading. A sand grain was  
56 observed to break into several particles followed by cracking in a second grain once the first  
57 grain was completely pulverized. Sand crushing changes the shape of sand grains, which, in  
58 return, affects the mechanical behaviour of sand. The term ‘morphology’ of sand is used to  
59 describe the external size and shape of the grains and fragments (Blott and Pye 2008). The  
60 morphology of sand grains affects its density, void ratio, shearing response, stiffness and  
61 coefficient of lateral stress (Yimsiri and Soga 1999; Latham et al. 2002; Cho et al. 2006; Guo  
62 and Stolle 2006; Tsomokos and Georgiannou 2010). Angular grains have lower crushing  
63 strength compared to round grains (Cheng et al. 2004; Gaurav et al. 2012). A numerical study  
64 (Ueda et al. 2013) showed that cleavage destruction, bending fracture, and edge abrasion were  
65 observed in circular or elliptical, elongated, and angular particles respectively. Sand crushing and  
66 the change in shape and grain size distribution reduces the permeability of sand by decreasing  
67 the internal pore space and altering the pore shape. Sand with irregular-shaped grains was shown  
68 to be 1.6~1.8 times less permeable than sand with round grains under gravity packing in a

69 numerical study using finite element flow simulation through internal pore structures (Garcia et  
70 al. 2009).

71 The oil and gas industry uses the ISO 13503-2 standard (2006) for testing the crushing  
72 characteristic of sand and to compare and select frac sand for hydraulic fracturing. However, this  
73 standard test only measures the percent of fines generated due to crushing under a specified  
74 compressive stress. The frac sand is not selected on the basis of other sand properties such as the  
75 stress-strain response, grain size gradation, and changes in sand grain shape as they are crushed.  
76 These properties are typically not measured during the standard crush test and are thus poorly  
77 understood. Furthermore, the impact of these factors on changes in the sand pack permeability is  
78 largely unknown. To address these issues, this paper uses an experimental approach to  
79 characterize the crushing characteristics and morphology change of frac sand from the Jordan  
80 Formation in Wisconsin, a popular source for frac sand with high roundness and good crushing  
81 resistance. The permeability reduction due to sand crushing is also interpreted. The results  
82 improve our understanding of the behaviour of Jordan frac sand under compression. This paper  
83 also demonstrates that more information can be extracted from the crushing test than is currently  
84 done, which can be used to optimize frac sand design to achieve a better sand pack permeability  
85 under field conditions.

## 86 **Jordan Formation Frac Sand**

### 87 *Geology description*

88 Sand used as a proppant in hydraulic fractures usually consists of highly pure quartz  
89 grains with ideal roundness and crushing resistance. In Wisconsin and Minnesota, frac sand is  
90 mined from four sandstone formations, namely the Middle and Upper Ordovician St. Peter  
91 Formation, the Upper Cambrian and Lower Ordovician Jordan Formation, the Cambrian Upper

92 Wonewoc Formation, and the Cambrian Mount Simon Formation. Figure 1 shows the  
93 distribution of these sandstone formations and the active/proposed frac sand mines and  
94 processing plants in Wisconsin. Among the four source formations, the Van Oser Member of the  
95 Jordan Formation has the highest percentage of desirable grain sizes (i.e., over 45% larger than  
96 mesh 40 by weight) and the lowest percentage of less desirable grain sizes (i.e., about 5%  
97 smaller than mesh 100 by weight) for hydraulic fracturing (Ostrom 1971).

98         The Jordan Formation is a marine sandstone that was deposited 500 million years ago.  
99 Outcrops of this formation were first described in streams and quarries near Jordan City,  
100 Minnesota by Winchell (1874). This sandstone was extensively studied by Runkel et al. (1994a,  
101 1994b, 2000, 2012). Chemical weathering is believed to have induced selective diagenetic  
102 leaching of plagioclase grains and other unstable minerals from the source rock for the sand that  
103 was eventually deposited. This created a mineralogically mature source area dominated by quartz  
104 grains (Odom's 1975, 1978). The sand was then carried by wind and rivers to shorelines located  
105 in Wisconsin, Minnesota and Northern Iowa. Abrasion in marine conditions as well as wind  
106 abrasion jointly created the textural maturity of the sand.

107         Two quartzose sandstone members are included in the Jordan Formation. The uppermost  
108 Van Oser Member consists of fine to medium-grained, cross-stratified, well-sorted, quartzose  
109 sandstone with 9 to 15 m thickness. The underlying Norwalk Member is a fine-grained,  
110 moderately sorted feldspathic sandstone with a thickness 15 to 18 m (Mudrey et al. 1987). The  
111 Van Oser is interpreted as a higher energy, marine intertidal sand while the Norwalk is as a low-  
112 energy, below wave base sand (Brown 2012).

113         The Jordan Formation is poorly cemented but does have some cement-like calcite, which  
114 may locally create tightly cemented aggregates so blasting is sometimes used to make the

115 sandstone more amenable to excavation. After excavation, the sandstone is crushed to recover  
116 the sand grains, which are then washed to remove fine particles such as silts and clays. The sand  
117 is then sent to a dryer and screening plant to sort the sand into desired sizes for hydraulic  
118 fracturing (Wisconsin Department of Natural Resources 2012).

### 119 *Grain size and microstructure*

120 The Jordan Formation frac sand used in this paper was washed in a processing plant near  
121 Plum City, Wisconsin, and then shipped to a drying and screening plant near Seven Persons,  
122 Alberta, for final processing. One of the most popular sizes of frac sand, mesh 20/40 as shown in  
123 Fig. 2, is used for this study. Mesh 20 and 40 is equivalent to 0.85 mm and 0.425 mm  
124 respectively. A mesh 20/40 sand means more than 90% of sand grain by weight is retained  
125 between 0.85 mm and 0.425 mm. A visual examination of the sand shows that most grains  
126 appear round and clean although some of the grain surfaces have a yellowish tone that may  
127 indicate a thin oxide coating. There are also occasional grains consisting of an agglomeration of  
128 smaller particles.

129 The grain size distribution for the 20/40 mesh size sand as received from the supplier was  
130 determined following the ASTM D6913 (2009) sieving standard. A 100 g representative sample  
131 of the sand under an air-dried condition was obtained and sieved with a 200 mm diameter metric  
132 sieve set on a shaker for 20 minutes. Table 1 shows the size distribution obtained by sieving. As  
133 expected for a 20/40 mesh sand, 80% of the sand grains by weight fall between sieve sizes of  
134 0.50 mm and 0.71 mm.

135 A Tescan Mira3 XMU field emission Scanning Electron Microscope (SEM) with 2 nm  
136 back-scattered electron resolution at 30 kV was used to investigate the microstructure of the  
137 natural and fractured sand grains.

138 Sand collected from a one-dimensional compression test to a maximum stress of 50 MPa  
139 was used to obtain the textures of natural grain surfaces and new fracture faces. The collected  
140 was sieved to four different sizes and then examined in a SEM. A sputtercoater was used to  
141 deposit a 10 nm thickness of a platinum-palladium alloy on the sand grains or particles to form a  
142 conductive surface.

143 As shown in Fig. 3, most sand grains from the 0.425 mm sieve remained unbroken  
144 although a few grains showed signs of abrasions or diametrical failures. For the 0.315 mm sieve,  
145 grains split in the middle were common and some cracks were present. Grains from the 0.16 mm  
146 sieve consisted of angular elongated fragments of sand grains. The smallest size fraction  
147 (0.08 mm sieve) consisted of more elongated fragments. New fracture faces and grain surfaces  
148 are easily distinguished from each other by their texture (smooth or rough).

### 149 **Crushing Characteristics of Frac Sand**

150 Sand crushing resistance and grain breakage characteristics affect the stress-strain  
151 response of sand and grain size degradation under compression, which is directly linked to sand  
152 pack permeability. It is also widely acknowledged that sand grains with different sizes might  
153 have different crushing strength (Nakata et al. 2001). To design a sand pack with higher crushing  
154 resistance and permeability, it is important to understand the crushing strength of different sand  
155 sizes and then to optimize the grain size distribution of the sand pack for different closure  
156 stresses.

157 One-dimensional compression tests were used to investigate the frac sand crushing  
158 characteristics. The crushing tests presented in this paper were performed on sand grains retained  
159 on 0.5 mm and 0.6 mm sieves respectively, because these are the major size components of mesh  
160 20/40 sand, the most commonly used size range for hydraulic fracturing. Ongoing research is

161 studying the crushing characteristics of other grain sizes including 0.71 mm, 0.425 mm and  
162 0.355 mm, and sand mixtures with different grain sizes but this work is beyond the scope of this  
163 paper. It should also be noted that the crushing tests were performed on dry sand without  
164 considering fluids or pore pressure. The sand used for the crushing test that came from a 0.5 mm  
165 sieve is termed as G500 sand, and G600 for sand from a 0.6 mm sieve.

### 166 *Test apparatus and procedure*

167 This test involves placing sand into a steel cup and then applying a compressive stress to  
168 the top of the sand with a steel loading piston as seen in Fig. 4. The testing apparatus were  
169 smaller than that used for the ISO 13503-2 standard to facilitate good acoustic emission  
170 monitoring while keeping the thickness of the sand in the cup similar to that in a real hydraulic  
171 fracture. The cup has a 25.4 mm inner diameter, 50.8 mm outer diameter, and is 70.28 mm deep.  
172 The loading piston is 25.4 mm in diameter and 80 mm long. A compression force was vertically  
173 applied to the piston using a Instron 3385H testing machine with a load capacity of 250 kN, load  
174 measurement accuracy of 0.5% down to 2.5 kN, and strain measurement accuracy of 0.5%. The  
175 loading rate was set to 0.1 mm/min to maintain a stress increase at less than 0.5 MPa/s. The  
176 stress applied to the sand pack in the cup and the resulting strain was measured at a rate of  
177 100 Hz during each test.

178 A 27 mm diameter piezoelectric sensor with a resonant frequency of 6.3 kHz was  
179 attached to the outside of the steel cup to record the sound created by sand grain fractures  
180 throughout the compression test. The sound from the crushing sand creates a voltage in the  
181 piezoelectric sensor, which was amplified and recorded at a rate of 25 kHz using a National  
182 Instruments USB-6210 data logger. A Fast Fourier transform was performed on the acoustic  
183 emission (AE) data recorded during the crushing tests. The waveforms detected by the

184 piezoelectric sensors were filtered to remove frequencies under 200 Hz, which were found to be  
185 associated with background noise. The grain breaking events have frequencies ranging between  
186 400 Hz to 8000 Hz.

187 For each crushing test,  $10 \pm 0.1$  g of sand was placed into the cup. The cup was placed  
188 onto a vibration table to level the sand surface and to achieve an approximately constant initial  
189 void ratio. The compressive stress applied to the sand in the crushing cup was up to 40 MPa to  
190 mimic the typical closure stresses in hydraulic fractures. The height of the sand in the steel cup  
191 was measured before the start of each crush test. These data were used to calculate the initial  
192 void ratio in the sand pack assuming that the quartz sand grains have a density of  $2.65 \text{ g/cm}^3$ .

193 The tests were repeated five times to evaluate inherent variability in the test data and to  
194 obtain a sufficient mass of sand for subsequent sieving. After each set of five tests, a sieve  
195 analysis was performed to determine the grain size distribution and the morphological properties  
196 of the crushed sand grains were analyzed.

### 197 *Test results*

198 After a compression test, the piston was removed from the cup and the sand grains inside  
199 the cup were observed with a microscope. A typical example of sand crushing due to  
200 compression is shown in Fig. 5. Diametrical failures in which a grain splits into two halves, can  
201 be seen at locations 1 to 3. At location 4 and 5, the split grains were further broken into many  
202 pieces of finer fragments. The white coloured particles of sand are fresh fines generated due to  
203 crushing.

204 The grain size distributions under applied stress levels of 10, 20, 30, and 40 MPa were  
205 obtained to understand the grain size variation with stress as shown in Fig. 6. The results reveal  
206 that sand crushing becomes significant once the compressive stress exceeds approximately

207 30 MPa. For crushing tests on G600 sand, at maximum compressive stresses of 30 and 40 MPa,  
208 14% and 29% of the original sand were respectively crushed to finer sizes and 2.7% and 11% of  
209 sand by weight respectively passed through a 0.355 mm sieve size. For crushing tests on G500  
210 sand under compressive stresses of 30 MPa and 40 MPa, 10% and 25% of the original sand were  
211 respectively crushed to finer size and 3.2% and 12% of sand by weight respectively passed  
212 through a 0.355 mm sieve. This indicates that sand particles in a size range of 0.355 to 0.425 mm  
213 were further crushed into even smaller fragments. Note that G600 sand shows a lower crushing  
214 resistance compared to G500 sand because more grains are crushed at a given stress level.

215 The stress-strain responses from five crush tests on G500 sand are shown in Fig. 7. From  
216 0 to 10 MPa, the stress carried by the G500 sand pack increased smoothly as the grains were  
217 compacted. There is a drop in the vertical stress around  $12.6 \pm 1.6$  MPa (mean  $\pm$  standard  
218 deviation using 5 tests) as shown in the stress-strain curves due to one or more grains breaking as  
219 verified with AE detection. This is similar to the one dimensional compression experiments by  
220 Hagerty et al. (1993) that indicated sand crushing began at an applied stress as low as 15 MPa.  
221 The stress increased with multiple small stress drops as further grains were broken especially  
222 when the stress exceeded 10 MPa, resulting in a zigzag shape for the stress-strain curve. It is also  
223 noted that the slope of the stress-strain curve became shallower and each drop in stress is less  
224 significant after 30 MPa compared to stresses from 10 to 30 MPa. The average one-dimensional  
225 constrained modulus of the sand pack at stresses between 15 and 25 MPa is  $485 \pm 27$  MPa while  
226 that between 32 and 38 MPa is  $250 \pm 31$  MPa. The decrease in the constrained modulus may be  
227 explained by the generation of smaller and more tabular sand fragments at compressive stresses  
228 in the range of 30 to 40 MPa as verified by the grain size distributions and the microscopic

229 morphology of the sand grains. The sand pack exhibits a less stiff response when these fragments  
230 are present and significant crushing of sand is occurring.

231 The positive values of the filtered AE voltage for Test 1 of G500 sand loaded up to  
232 40 MPa compressive stress are presented in Fig. 8. The voltage spikes and stress drops are  
233 coincident with each other. For example, a voltage spike larger than 3 V occurs at approximately  
234 11.5 MPa corresponding to the first large drop in stress. This shows that the stress drop was  
235 caused by grain breaking. The larger voltage spikes ( $>1$  V) occur between compressive stresses  
236 of 10 and 30 MPa. The voltage spikes occurring when the stress was between 30 and 40 MPa are  
237 typically smaller than 1 V. The smaller AE signals that occur at higher stress levels might be  
238 explained by the evolving nature of the grain size distribution under different stresses. As shown  
239 in Fig. 6, only 3.5% of G500 sand was crushed to finer particles under a compressive stress of  
240 20 MPa. Most of these fragments remained on sieve sizes of 0.355 mm and 0.425 mm, indicating  
241 that the initial sand crushing was dominated by grains being split into two halves. The creation of  
242 small sand particles as the compressive stress increased may increase the number of contact  
243 points among the grains or fragments and thus more evenly distribute the contact forces. This in  
244 turn may result in smaller energy releases during subsequent crushing and thus lower voltage  
245 spikes.

246 For G600 sand, the stress applied to the sand increased smoothly and then experienced its  
247 first drop at a compressive stress around 9.6 MPa ( $\pm$  std. dev. 1.7 MPa using 5 tests) as seen in  
248 Fig. 9, which is slightly lower compared with G500 sand ( $12.6 \pm 1.6$  MPa). This may be  
249 explained by larger size grains having a lower strength than the smaller size grains since more  
250 defects are likely in a bigger sand grain. The average one-dimensional constrained modulus at  
251 stresses between 15 and 25 MPa is  $467 \pm 44$  MPa while that between 32 and 38 MPa is  $221 \pm$

252 31 MPa. The average one-dimensional constrained modulus of G600 sand under lower stress  
253 levels (15 to 25 MPa) is similar to G500 sand. This may be because the degree of sand crushing  
254 is similar for the two sand sizes at this stress level. At a higher stress the sand pack consisting of  
255 the larger G600 sand grains had a lower modulus than G500 sand. The compressive stress and  
256 AE voltage versus time for Test 2 of G600 sand are presented in Fig. 10. A spike with voltage  
257 larger than 2.1 V occurs at approximately 9 MPa when the first large stress drop occurred. This  
258 further shows that the stress drop was caused by grain breaking. Voltage spikes that are larger  
259 than 1 V occur between compressive stresses of 9 and 25 MPa, while voltage amplitudes at  
260 stresses between 25 to 40 MPa were typically lower than 1 V.

261 An attempt was made to count the number of individual AE events that occurred during  
262 each crush test. The approach suggested by Zhao et al. (2013) was used for this purpose. AE  
263 readings with a voltage higher than a threshold of 0.02 V were first determined and then those  
264 readings which occurred within an event duration 0.03 s were counted as a single crushing event.  
265 The AE voltage and the AE event count are plotted versus the strain in Figs. 8 and 10 for tests on  
266 G500 and G600 sand. For the G500 sand, the number of AE events increased slowly to  
267 approximately 300 at 25 MPa and then more quickly to just over 1000 events at 40 MPa. For  
268 G600 sand, the number of AE events increased slowly to around 360 at 25 MPa and then  
269 dramatically to 1450 at 40 MPa. The AE event rate is defined as the number of AE events per  
270 every 2% vertical strain of the sand pack. As shown in Figs. 8 and 10, the AE event rate of G500  
271 sand increases from about 50 events/2% strain at 10 MPa to about 200 events/2% strain at  
272 stresses between 25 to 40 MPa. For G600 sand, the AE event rate increases from about 50  
273 events/2% strain near 10 MPa to 300 events/2% strain at stresses between 25 to 40 MPa.

274 Consistent with the grain size data, the number of AE events and the AE event rate both indicate  
275 that more grains of G600 sand were broken than G500 sand under the same stress levels.

276 To compare the crushing strength of the Jordan Formation frac sand with other kinds of  
277 sand, the Hardin relative breakage ( $B_r$ ) of G500 and G600 sand was calculated based on the grain  
278 size distribution (Hardin 1985). The values for  $B_r$  are plotted in Fig. 11, where they are compared  
279 with data from Coop and Lee (1993) for well sorted the Dogs Bay sand ( $D_{50} = 0.28$  mm) and the  
280 Ham River sand ( $D_{50} = 0.227$  mm), and from Vilhar et al. (2013) for Bostanj silty sand ( $D_{50} =$   
281 0.11 mm). The data from the one-dimensional tests have been plotted by assuming  $\phi' = 34^\circ$  and  
282  $K_\theta = 1 - \sin\phi'$  for calculating the mean stress ( $p'$ ). The G500 has slightly lower values of  $B_r$  than  
283 the G600 under the same stress level. The G600 and G500 sand exhibit much lower breakage  
284 than the Dogs Bay sand and the Ham River sand, while the sand has similar breakage to the  
285 Bostanj silty sand. It should be noted that G600 and G500 have a much higher  $D_{50}$  than the  
286 Bostanj silty sand, which implies the crushing resistance of the Jordan Formation sand is higher  
287 than the Bostanj silty sand assuming the crushing strength increases with the decrease of the  
288 grain size. Based on the shift in the gradient of the stress-strain curves in Figs. 7 and 9 and the  
289 void ratio versus stress curve in Fig. 12. G500 and G600 has a yield point at around 27.8 MPa  
290 and 24.8 MPa respectively. These are higher than yield stress of a silica sand (11.6 MPa for size  
291 0.61~0.71 mm; 16.9 MPa for size 0.25~0.3 mm) and close to that of glass ballotini (26.5 MPa for  
292 size 0.85~1.0 mm) as reported by Nakata et al. (2001) for one-dimensional compression test  
293 results.

## 294 **Morphology Change of Sand Grains Due to Crushing**

295 Sand crushing changes the grain shape and size, which affects the mechanical behaviour  
296 and permeability of the sand pack. A comprehensive analysis using images of the grains or

297 fragments captured by a microscope was conducted to characterise sand particle size and shape  
298 before and after the crushing tests. An optical Zeiss Stereo Discovery.V8 microscope with a  
299 build-in camera (AxioCam ICC1) was used to examine the sand grains. The microscope  
300 objective lens has a magnification from 25x to 200x. The sand was placed into a plastic petri dish  
301 with a black bottom while the lighting was from above. Grains were separated carefully to avoid  
302 grain overlap or touching before images were captured. A calibration slide was used to calibrate  
303 the scale of the field of view.

304 ImageJ software (Schneider et al. 2012) was used to perform a morphology analysis of  
305 the grains. ImageJ is a Java-based image processing program with user-defined plugins and  
306 recordable macros. Measurements for each individual particle were evaluated from its image and  
307 results were filtered by particle size and circularity. Several 2D particle shape descriptors are  
308 used. These include the 2D area ( $A$ ) and perimeter ( $P$ ) of each grain. Sphericity ( $S$ ) and  
309 roundness ( $R$ ) of the grain make use of the calculated area and perimeter and are defined in  
310 Equations 1 and 2 and have a maximum value of 1 for circles. For a square,  $R = 0.785$  while  $S =$   
311 1. The major axis was found for the best fit ellipse with the same area, orientation, and centroid  
312 to the original shape as shown in Fig. 13. The maximum Feret diameter ( $MaxFeret$ ) is the  
313 maximum distance between two parallel tangents touching the outline of a grain. The minimum  
314 Feret diameter ( $MinFeret$ ) corresponds to the minimum distance which is similar to a caliper  
315 diameter. The ratio of  $MinFeret$  and  $MaxFeret$  is the aspect ratio ( $AR$ ). The roughness parameter  
316  $R$  used in this paper describes overall roughness while that defined by Krumbein and Sloss  
317 (1963) is more focused on local sharpness using a few sharpest corners, which is a scale-  
318 dependent parameter. The meaning of  $R$  and  $S$  values can be appreciated by reference to Fig. 14,  
319 which is a plot of representative quartz particles retained on sieve sizes from 0.08 mm to 0.5 mm.

$$R = \frac{4\pi A}{P^2} \quad (1)$$

$$S = \frac{4A}{\pi(\text{major axis})^2} \quad (2)$$

$$AR = \frac{\text{MinFerret}}{\text{MaxFerret}} \quad (3)$$

### 323 *Morphology of original sand*

324 Two hundred grains of G500 sand were randomly selected for morphology analysis. The  
 325 mean *MinFerret* was  $0.645 \pm 0.049$  mm. The mean value of *MinFerret* is a slightly larger than the  
 326 finest sieve size that the G500 sand passed through, which is 0.6 mm. This is in good agreement  
 327 with results by Altuhafi et al. (2012) since the sieve size that grains can pass through depends on  
 328 both the intermediate and minimum grain dimensions. The aspect ratio was  $0.776 \pm 0.085$ , the  
 329 roundness was  $0.848 \pm 0.030$  and the sphericity was  $0.783 \pm 0.096$ .

330 Fig. 15 shows the correlation of sphericity and roundness with aspect ratio for G500 sand.  
 331 Most grains have a roundness of 0.8 to 0.9 and a sphericity between 0.65 and 0.95. Grains tend  
 332 to have a higher sphericity and aspect ratio as the roundness increases. Mathematically, the ratio  
 333 of sphericity and roundness is equal to the square of the actual perimeter over the perimeter of a  
 334 circle with a diameter equal to the major axis. For most grains, the major axis of the best fit  
 335 ellipse is close to the maximum Feret diameter. The resulting perimeter of a circle with a  
 336 diameter equal to the major axis will be larger than the grain perimeter. However, some sand  
 337 grains with a high aspect ratio ( $>0.9$ ) and concave surfaces will result in a higher sphericity  
 338 compared to the roundness.

339 The morphology analysis was repeated on 200 randomly sampled grains of G600 sand  
 340 and the results are shown in shown in Fig. 16. The *MinFerret* was  $0.757$  mm  $\pm$   $0.060$  mm. Again,

341 the mean value of the minimum Feret diameter is slightly larger than the finest sieve size that the  
342 G600 sand passed through, which is 0.71 mm. The aspect ratio was  $0.792 \pm 0.081$ , the roundness  
343 was  $0.852 \pm 0.029$ , and the sphericity was  $0.798 \pm 0.092$ . Compared to G500 sand, the G600  
344 sand grains are closer to circular shapes, and have a slightly lower standard deviation in these  
345 three descriptors.

#### 346 *Morphology of sand from crush tests*

347 After 40 MPa crushing tests were performed, the sand was sieved into different size  
348 ranges. The grains retained on each sieve were used for morphology analysis. As shown in Fig.  
349 17, sand grains retained on a 0.5 mm sieve remain unbroken and have high sphericity and  
350 roundness. Sand particles from 0.425 mm, 0.355 mm and 0.3 mm sieves, typically consist of  
351 grains that have been split into two or more fragments. Elongated or tabular particles were more  
352 common for the small sand fragments collected on sieves finer than 0.3 mm in size.

353 For morphology analysis, 100 grains from each sieve were randomly selected. The grains  
354 collected from the 0.5 mm sieve had a slightly higher mean roundness (0.842), sphericity (0.834)  
355 and aspect ratio (0.821) than the original G500 sand prior to the crushing test. Likewise, the  
356 grains collected from the 0.6 mm sieve had a slightly higher mean roundness (0.853), sphericity  
357 (0.811) and aspect ratio (0.803) than the original G600 sand. These results indicated that rounder  
358 and more spherical grains tend to stay unbroken under compression. For particles collected from  
359 the 0.08 mm sieve, the aspect ratio was 0.570 for G500 sand and 0.615 for G600 sand, which  
360 means the maximum Feret diameter was almost two times of the minimum Feret diameter  
361 indicating an elongated grain shape. As the sieve size reduces, the mean value of roundness,  
362 sphericity and aspect ratio also decrease as seen in Figs. 18 and 19. The mean value of minimum  
363 Feret diameter of grains from each sieve has a nearly linear relation with the sieve size. This may

364 imply that the ratio of the intermediate and minimum grain dimension remains similar for each  
 365 grain size.

### 366 **Permeability Reduction Due to Sand Crushing**

367 The widely used empirical Kozeny-Carman equation combined with the Hazen formula  
 368 (Chapuis 2004, Göktepe and Sezer 2010) can be used to estimate the permeability of the sand  
 369 pack. The permeability ( $k$ ) is expressed as:

$$370 \quad k = C \times \frac{e^3}{1+e} \times D_{10}^2 \quad (4)$$

371 where,  $C$  is the constant depending on the geometry of pore channels,  $e$  is the sand pack void  
 372 ratio,  $D_{10}$  is the diameter at which the 10% of the particles are finer by weight.

373 A permeability reduction factor ( $k_r$ ) is defined here as the ratio of permeability after and  
 374 before crushing, which can be expressed as:

$$375 \quad k_r = \frac{e_2^3 (1+e_1)}{e_1^3 (1+e_2)} \times \frac{D_{10,2}^2}{D_{10,1}^2} \quad (5)$$

376 where the subscripts 1 and 2 are the value of each parameter before and after crushing  
 377 respectively.

378 For comparison, a generalised Kozeny-Carman equation considering the particle shape  
 379 (Carrier 2003) can be used to estimate the influence of grain morphology on permeability. The  
 380 permeability ( $k'$ ) is expressed as:

$$381 \quad k' = \frac{1}{C_{K-C}} \times \frac{e^3}{1+e} \times \frac{D_{eff}^2}{SF^2} \quad (6)$$

382 where  $C_{K-C}$  is an empirical coefficient,  $SF$  is a unitless grain shape factor, and  $D_{eff}$  is the effective  
 383 diameter that is given as:

$$384 \quad D_{eff} = \frac{1}{\sum_i (f_i / (D_{li}^{0.404} D_{si}^{0.595}))} \quad (7)$$

385 where  $f_i$  the percentage of particles retained between two sieve sizes, the larger sieve  $D_{li}$  and the  
 386 smaller sieve  $D_{si}$ .

387 Likewise, a permeability reduction ( $k_r'$ ) can be expressed as:

$$388 \quad k_r' = \frac{e_2^3 (1 + e_1)}{e_1^3 (1 + e_2)} \times \frac{D_{eff,2}^2}{D_{eff,1}^2} \times \frac{SF_1^2}{SF_2^2} \quad (8)$$

389 where the subscripts 1 and 2 are the value of each parameter before and after crushing  
 390 respectively.

391 The void ratio can be interpreted from the sand pack height that was measured during the  
 392 crush tests. The decrease in the void ratio with compressive stress is shown in Fig. 12 for two  
 393 typical tests. The void ratios for the G500 sand and G600 sand packs decrease in a similar  
 394 manner. The higher the compressive stress, the more significant the void ratio decrease. The  
 395 values of  $D_{10}$  and  $D_{eff}$  for each stress interval can be obtained from the grain size distributions  
 396 obtained by sieve analysis.

397 At 10 MPa increments in the compressive stress, the values of the shape factor  $SF$  were  
 398 estimated using the suggestion by Fair and Hatch (1933) for different grain shapes. The value of  
 399  $SF$  is 6.1 for the original sand (0 MPa) as grain shapes are nearly round, 6.4 for sand loaded to 10  
 400 and 20 MPa because a small portion of grains are abraded and split, 7.4 for sand loaded to  
 401 30 MPa because a significant portion of the grains are split, and 7.7 for 40 MPa because many  
 402 grains are split and fragments are further crushed into angular shapes.

403 Using the empirical equations and the data in Table 2, the calculated permeability  
404 reduction for each stress level is shown in Fig. 20. The values given by Equations 5 and 8 are  
405 close to each other although the generalised Kozeny-Carman equation (Equation 8) tends to give  
406 slightly lower values. As the stress increases from 0 to 40 MPa, the permeability reduces by up  
407 to one order of magnitude. The permeability reduction at stress levels less than 20 MPa is mainly  
408 caused by a decrease in void ratio due to grain position realignment due to compaction. The  
409 permeability reduction at compression stresses larger than roughly 20 to 30 MPa is caused by  
410 decreases in both void ratio and grain diameter as well as changes in the grain shape. Ignoring  
411 the grain size, round grains are 1.6 times,  $(SF_{round}/SF_{angular})^2 = (7.7/6.1)^2$ , more permeable than  
412 angular grains, which matches a numerical study using finite element flow simulation through  
413 internal pore structures (Garcia et al. 2009). Although the permeability reduction factor for a  
414 G500 sand pack is similar to G600 sand at the same stress, G600 sand is 1.4 times more  
415 permeable than G500 sand under 0 to 20 MPa compressive stress and 1.3 times more permeable  
416 under 40 MPa compressive stress. So while the G600 sand experiences more crushing and fines  
417 generation than the G500 sand, the larger initial grain size more than compensates for the  
418 presence of the fines in terms of the resulting permeability through the sand pack.

419 Permeability tests by Coulter et al. (1972) found that 5% fines can cause more than a  
420 50% reduction in proppant pack permeability for mesh 20/40 sand under a compressive stress of  
421 24.1 MPa. The tests in this paper give a similar result. As shown in Fig. 20, the permeability  
422 reduces by about 50% for both G500 and G600 sand tested under 20 MPa compression. At this  
423 stress, 3.5% and 5% of the sand grains are crushed respectively, while the sand pack height  
424 decreases by 6 to 7% due to compression as seen from Figs. 7 and 9. The resulting sand pack

425 conductivity in a hydraulic fracture (sand pack permeability  $\times$  sand pack height) is estimated to  
426 reduce by about 50%.

## 427 **Conclusions**

428 This paper examines the crushing characteristics and morphological changes of Jordan  
429 Formation sand subjected to varying levels of stress in one-dimensional constrained compression  
430 tests. When the effective stresses applied to a sand pack exceed roughly 10 MPa grain crushing  
431 initiates and when stresses exceed roughly 30 MPa a significant portion of the quartz grains are  
432 crushed. Acoustic emissions caused by grain breaking were directly associated with drops in the  
433 compressive stress. With further increase in compressive stress, a zigzag stress-strain response is  
434 observed as sand grains break and the sand becomes more compacted. The overall sand pack  
435 stress-strain response becomes softer as grains are crushed, especially at stress levels above  
436 roughly 30 MPa. Since G600 sand experiences more grain crushing than G500 sand it also has a  
437 softer stress-strain response than G500 sand at the higher stress levels.

438 The sand grain shape or morphology was characterized by measurements of particle  
439 roundness, sphericity, and aspect ratio. Most sand grains from the original Jordan Formation  
440 sand have a roundness of 0.8 to 0.9 and a sphericity of 0.65 to 0.95. The sand grains are  
441 generally close to spherical in shape, which is desirable for frac sands. Sand grains analysed after  
442 being compressed to 40 MPa show that the uncrushed grains have a higher mean value of  
443 roundness and sphericity than values before the crushing test. This suggests that more spherical  
444 grains have a higher crushing resistance. Crushed sand collected from finer sieve sizes have  
445 mean values of roundness, sphericity and aspect ratio that decrease as the particle becomes  
446 smaller. The shape of the particles shifts from nearly spherical grains to diametrically split grains  
447 and then to small, elongated and angular fragments for the smaller particle sizes.

448           The Kozeny-Carman empirical equations were used to estimate the permeability through  
449 a sand pack as a function of the measured particle size, particle shape, and void ratio. The results  
450 show that the permeability for sand under 20 MPa compression reduces by more than 40%  
451 compared to initial conditions. This is mainly caused by a decrease in void ratio due to  
452 compaction. The permeability reduces by over 80% at a 40 MPa stress, which is jointly caused  
453 by void ratio decrease and sand crushing. It is important to note that the permeability reduction  
454 that occurs as the sand is crushed is associated with three factors: reduction in void ratio,  
455 reduction in particle size, and a shift away from spherical particle shapes.

456           G600 sand is predicted to be 1.3 to 1.4 times more permeable than G500 sand under  
457 compressive stresses of 10 to 40 MPa because the average grain size of the sand pack is larger  
458 despite a tendency for G600 sand to crush more easily.

459           This paper demonstrates that frac sand selection based only on sand crushing percentage  
460 is not sufficient to achieve a higher permeability. Instead, it is recommended that the influence of  
461 grain size reduction, changes in particle shape, and reduction in void ratio be evaluated to better  
462 understand the sand pack permeability in a hydraulic fracture at depth. For this purpose, a  
463 methodology for conducting a more comprehensive assessment of frac sand permeability using  
464 easily obtained data from standard crush tests is presented. This methodology does not rely on  
465 conducting permeability tests in the laboratory. Instead, the geometric characteristics of the  
466 crushed sand are measured and used to predict the permeability using widely accepted empirical  
467 equations.

## Acknowledgments

This work was supported by grants from Mitacs and the British Columbia Oil and Gas Commission. The financial support from a university fellowship and the China Scholarship Council to the first author is also gratefully acknowledged.

## References

- Altuhafi, F., O'Sullivan, C., and Cavarretta, I. 2012. Analysis of an image-based method to quantify the size and shape of sand particles. *Journal of Geotechnical and Geoenvironmental Engineering*, **139**(8): 1290-1307.
- ASTM D6913 2009. Standard test methods for particle-size distribution gradation of soils using sieve analysis, ASTM D6913 - 042009e1.
- Benson, M.E., and Wilson, A.B. 2015. Frac sand in the United States - A geological and industry overview: U.S. Geological Survey Open-File Report 2015-1107, 78 p., <http://dx.doi.org/10.3133/ofr20151107> [cited 20 November 2015].
- Blott, S.J., and Pye, K. 2008. Particle shape: a review and new methods of characterization and classification. *Sedimentology*, **55**(1): 31-63.
- Brown, B. 2012. Hydrofrac sand in Wisconsin. Wisconsin Geological and Natural History Survey. Available from [http://monroe.uwex.edu/files/2012/02/Frac\\_sand\\_in\\_Wisconsin1.pdf](http://monroe.uwex.edu/files/2012/02/Frac_sand_in_Wisconsin1.pdf) [cited 20 November 2015].
- Carrier III, W.D. 2003. Goodbye, Hazen; Hello, Kozeny-Carman. *Journal of Geotechnical and Geoenvironmental Engineering*, **129**(11): 1054-1056.
- Chapuis, R.P. 2004. Predicting the saturated hydraulic conductivity of sand and gravel using effective diameter and void ratio. *Canadian Geotechnical Journal*, **41**(5): 787-795.

- Cheng, Y.P., Bolton, M. D., and Nakata, Y. 2004. Crushing and plastic deformation of soils simulated using DEM. *Géotechnique*, **54**(2): 131-141.
- Cho, G.C., Dodds, J., and Santamarina, J.C. 2006. Particle shape effects on packing density, stiffness, and strength: natural and crushed sands. *Journal of Geotechnical and Geoenvironmental Engineering*, **132**(5): 591-602.
- Chuhan, F.A., Kjeldstad, A., Bjørlykke, K., and Høeg, K. 2002. Porosity loss in sand by grain crushing - experimental evidence and relevance to reservoir quality. *Marine and Petroleum Geology*, **19**(1): 39-53.
- Coop, M.R. and Lee, I.K. 1993. The behaviour of granular soils at high stresses. In *Predictive Soil Mechanics: Proceedings of the Wroth Memorial Symposium on predictive soil mechanics*, pp. 186–198.
- Coop, M.R., Sorensen, K.K., Freitas, T.B., and Georgoutsos, G. 2004. Particle breakage during shearing of a carbonate sand. *Géotechnique*, **54**(3): 157-163.
- Coulter, G.R., and Wells, R.D. 1972. The advantages of high proppant concentration in fracture stimulation. *Journal of Petroleum Technology*, **24**(6): 643-650.
- Fair, G.M., and Hatch, L.P. 1933. Fundamental factors governing the stream-line flow of water through sand. *Journal of American Water Works Association*, **25**(11): 1551-1565.
- Garcia, X., Akanji, L.T., Blunt, M.J., Matthai, S.K., and Latham, J.P. 2009. Numerical study of the effects of particle shape and polydispersity on permeability. *Physical Review E*, **80**(2), 021304.
- Gaurav, A., Dao, E.K., and Mohanty, K.K. 2012. Evaluation of ultra-light-weight proppants for shale fracturing. *Journal of Petroleum Science and Engineering*, **92**: 82–88.

- Ghafghazi, M., Shuttle, D.A., and DeJong, J.T. 2014. Particle breakage and the critical state of sand. *Soils and Foundations*, **54**(3): 451-461.
- Göktepe, A.B., and Sezer, A. 2010. Effect of particle shape on density and permeability of sands. *Proceedings of the ICE-Geotechnical Engineering*, **163**(6): 307-320.
- Guo, P.J., and Stolle, D.F.E. 2006. Fabric and particle shape influence on  $k_0$  of granular materials. *Soils and Foundations*, **46**(5): 639-652.
- Hagerty, M., Hite, D., Ullrich, C., and Hagerty, D. 1993. One-dimensional high-pressure compression of granular media. *Journal of Geotechnical Engineering*, **119**(1): 1-18.
- Hardin, B.O. 1985. Crushing of soil particles. *Journal of Geotechnical Engineering*, **111**(10): 1177-1192.
- ISO 13503-2:2006. Petroleum and natural gas industries - Completion fluids and materials - Part 2: Measurement of properties of proppants used in hydraulic fracturing and gravel-packing operations.
- Krumbein, W.C., and Sloss, L.L. 1963. *Stratigraphy and sedimentation*, 2nd Ed., Freeman, San Francisco.
- Kurz, B.A., Schmidt, D.D., and Cortese, P.E. 2013. Investigation of improved conductivity and proppant applications in the Bakken formation. In *SPE Hydraulic Fracturing Technology Conference*. Society of Petroleum Engineers.
- Lacy, L.L., Rickards, A.R., and Ali, S.A. 1997. Embedment and fracture conductivity in soft formations associated with HEC, borate and water-based fracture designs. In *SPE Annual Technical Conference and Exhibition*. Society of Petroleum Engineers.
- Lade, P.V., Yamamuro, J.A., and Bopp, P.A. 1996. Significance of particle crushing in granular materials. *Journal of Geotechnical Engineering*, **122**(4): 309-316.

- Latham, J.P., Munjiza, A., and Lu, Y. 2002. On the prediction of void porosity and packing of rock particulates. *Powder Technology*, **125**(1): 10-27.
- Luzzani, L., and Coop, M.R. 2002. On the relationship between particle breakage and the critical state of sands. *Soils and Foundations* **42**(2): 71-82.
- Mudrey, M.G. LaBerge, Jr., Myers, P.E., and Cordua, W.S. 1987. Bedrock geology of Wisconsin: Northwest sheet. University of Wisconsin-Extension, Geological and Natural History Survey.
- Nakata, Y., Hyde, A., Hyodo, M., and Murata, H. 1999. A probabilistic approach to sand particle crushing in the triaxial test. *Géotechnique*, **49**(5): 567-583.
- Nakata, Y., Kato, Y., Hyodo, M., Hyde, A., and Murata H. 2001. One-dimensional compression behaviour of uniformly graded sand related to single particle crushing strength. *Soils and Foundations*, **41**(2): 39-51.
- Odom, I.E. 1975. Feldspar-grain size relations in Cambrian arenites, Upper Mississippi Valley. *Journal of Sedimentary Petrology*, **45**(3): 636-650.
- Odom, I.E. 1978. Mineralogy of Cambrian sandstones, upper Mississippi Valley: Wisconsin Geological and Natural History Survey Field Trip Guidebook 3, p. 23-45.
- Ostrom, M.E., 1971, Preliminary Report on Results of Physical and Chemical Tests of Wisconsin Silica Sandstones: Wisconsin Geological and Natural History Survey Information Circular 18, 61p.
- Palisch, T.T., Duenckel, R. J., Chapman, M. A., Woolfolk, S., and Vincent, M. C. 2009. How to use and misuse proppant crush tests - exposing the top 10 myths. In SPE Hydraulic Fracturing Technology Conference. Society of Petroleum Engineers.

- Parab, N.D., Claus, B., Hudspeth, M.C., Black, J.T., Mondal, A., Sun, J., Fezzaa, K., Xiao, X., Luo, S.N., and Chen, W. 2014. Experimental assessment of fracture of individual sand particles at different loading rates. *International Journal of Impact Engineering*, **68**: 8-14.
- Romanson, R., Riviere, N., Taylor, B., McIntosh, G., Wilson, M., Loran, C., and Cockbill, J. 2010. Montney fracturing-fluid considerations: case history. In *Canadian Unconventional Resources and International Petroleum Conference*. Society of Petroleum Engineers.
- Runkel, A.C. 1994a. Deposition of the uppermost Cambrian Croixan Jordan Sandstone, and the nature of the Cambrian–Ordovician boundary in the upper Mississippi Valley: *Geological Society of America Bulletin* **106**: 492–506.
- Runkel, A.C. 1994b. Revisions to the stratigraphic nomenclature of the Jordan Sandstone, upper Mississippi Valley region: *Shorter contributions to the Minnesota Geological Survey Report of Investigations* **43**, p. 60–71.
- Runkel, A.C. 2000. Sedimentology of the Upper Cambrian Jordan Sandstone—A classic cratonic sheet sandstone deposited during regression in a “typical” marine setting, *Guidebook for 30th Annual Field Conference, Great Lakes Section for the Society for Sedimentary Geology*, p. 43-46.
- Runkel, A.C., Syverson, K., Steenberg, J., Bendernagel, M., Bauer, A., Kent, A., Thompson, M., Stauffer, T., and Brown, B., eds. 2012. Field guidebook on the silica sand resources of western Wisconsin, *Conference on the silica sand resources of Minnesota and Wisconsin, Precambrian Research Center Guidebook 12-01: Brooklyn Park, Minnesota*, 45 p.
- Schneider, C.A., Rasband, W. S., and Eliceiri, K. W. 2012. NIH Image to ImageJ: 25 years of image analysis. *Nature Methods*, **9**: 671–675.

- Song, L., and Hareland, G. 2012. Minimum horizontal stress profile from logging data for Montney Formation of North East British Columbia. In SPE Canadian Unconventional Resources Conference, Society of Petroleum Engineers.
- Terzaghi, K. and Peck, R.B. 1948. Soil mechanics in engineering practice. John Wiley, New York.
- Tsomokos, A., and Georgiannou, V.N. 2010. Effect of grain shape and angularity on the undrained response of fine sands. *Canadian Geotechnical Journal*, **47**(5): 539-551.
- Ueda, T., Matsushima, T., and Yamada, Y. 2013. DEM simulation on the one-dimensional compression behavior of various shaped crushable granular materials. *Granular Matter*, **15**(5): 675-684.
- Vilhar, G., Jovičić, V., & Coop, M.R. 2013. The role of particle breakage in the mechanics of a non-plastic silty sand. *Soils and Foundations*, **53**(1), 91-104.
- Winchell, N.H. 1874. The geology of the Minnesota Valley, part e The Jordan Sandstone: Geological and Natural History Survey of Minnesota, Second Annual Report, p. 147-152.
- Wisconsin Department of Natural Resources. 2012. Silica Sand Mining in Wisconsin. Available from <http://dnr.wi.gov/topic/mines/documents/silicasandminingfinal.pdf> [cited 20 November 2015].
- Wisconsin Geological and Natural History Survey. 2014. Frac sand in Wisconsin. Available from <http://wgnhs.uwex.edu/pubs/fs05/> [cited 20 November 2015].
- Yimsiri, S., and Soga, K. 1999. Effect of surface roughness on small-strain modulus: micromechanics view. *Pre-failure Deformation Characteristics of Geomaterials*, **1**: 597-602.
- Zhang, X., and Baudet, B.A. 2013. Particle breakage in gap-graded soil. *Géotechnique Letters*, **3**: 72-77.

Zhao, X., Cai, M., Wang, J., and Ma, L. 2013. Damage stress and acoustic emission characteristics of the Beishan granite. *International Journal of Rock Mechanics and Mining Sciences*, **64**, 258-269.

Draft

Table 1. Grain size distribution of mesh 20/40 sand

Sieve size (mm)	1.0	0.85	0.71	0.6	0.5	0.425	0.355	0.3
(mesh No.)	(18)	(20)	(25)	(30)	(35)	(40)	(45)	(50)
Weight percent retained	0	2.4	12.4	37.9	42.1	4.9	0.3	0

Table 2. Parameters for permeability reduction estimation using empirical equations

Stress (MPa)	G500 sand				G600 sand			
	$e$	$D_{10}$	$D_{eff}$	$SF$	$e$	$D_{10}$	$D_{eff}$	$SF$
0	0.658	0.60	0.539	6.1	0.655	0.71	0.643	6.1
10	0.597	0.53	0.536	6.4	0.597	0.62	0.634	6.4
20	0.561	0.515	0.530	6.4	0.561	0.61	0.628	6.4
30	0.521	0.50	0.508	7.4	0.517	0.575	0.593	7.4
40	0.454	0.30	0.443	7.7	0.444	0.325	0.516	7.7

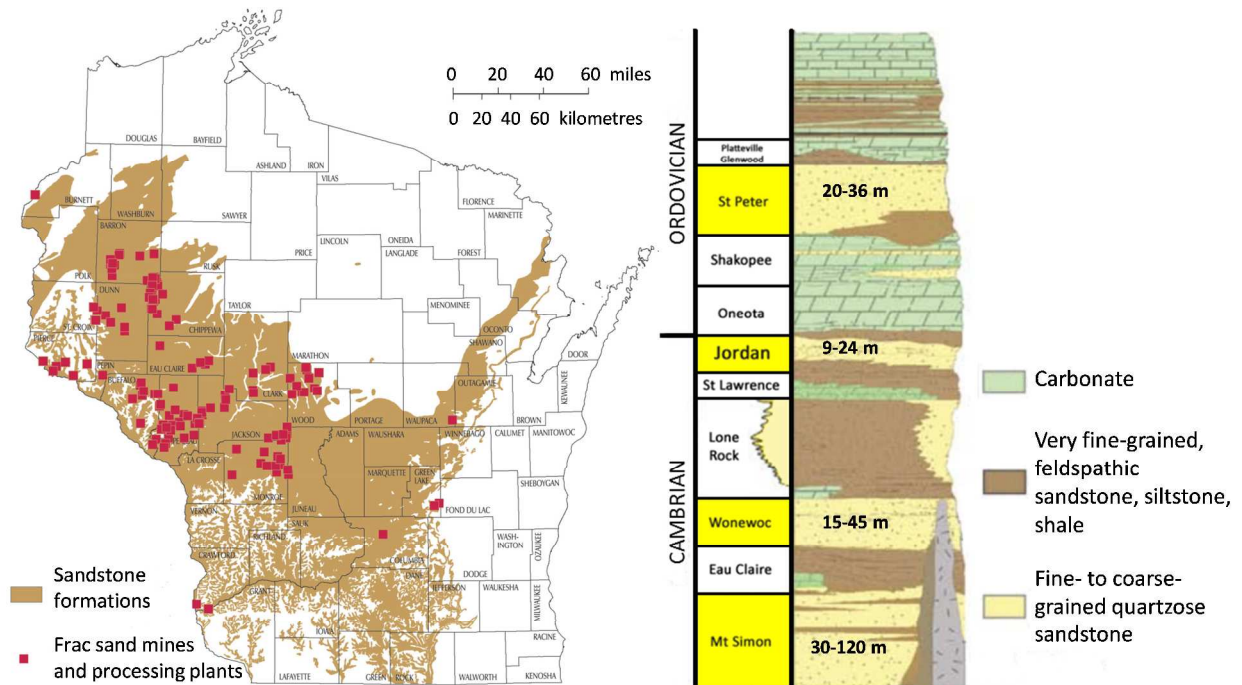


Fig 1. Frac sand mines and sandstone formations in Wisconsin and typical geological section (Modified from Wisconsin Geological and Natural History Survey 2014, and Runkel et al. 2012)



Fig 2. Mesh 20/40 Jordan frac sand

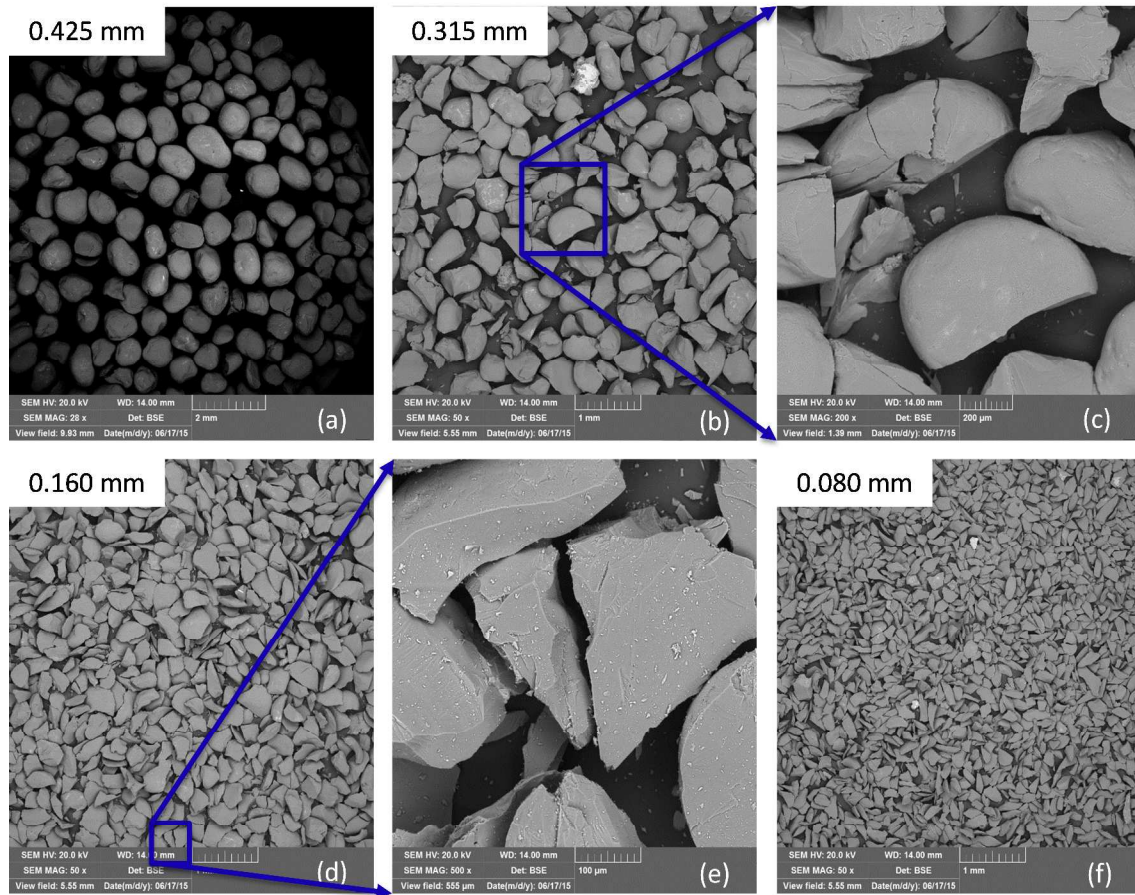


Fig 3. SEM images of sand grains from different sieve sizes

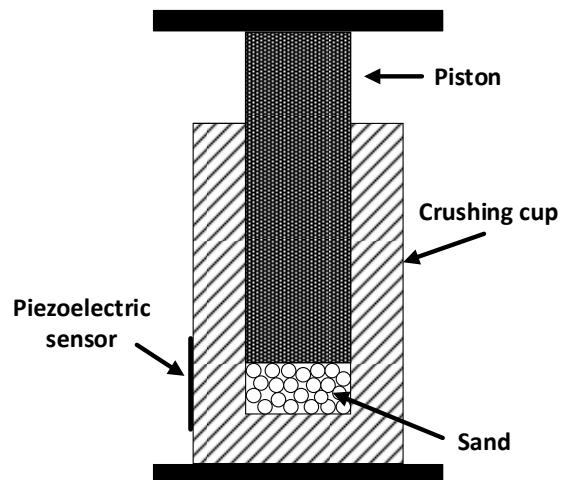


Fig 4. Steel cup and piston used for a one-dimensional compression test

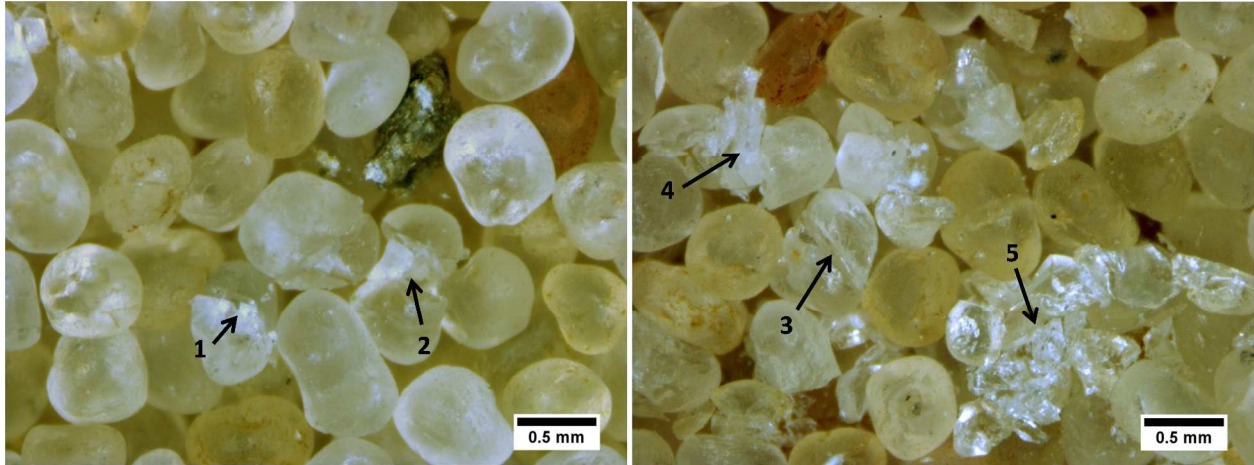


Fig 5. Crushed and intact sand grains after 30 MPa (left) and 40 MPa (right) compression

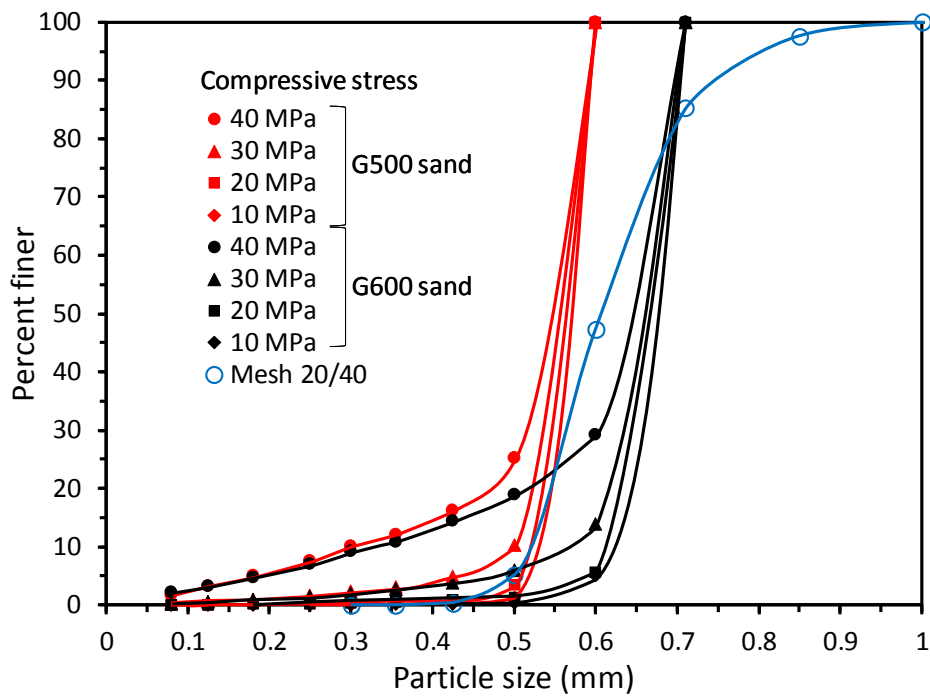


Fig 6. Grain size distributions of G500 and G600 sand under different stress levels

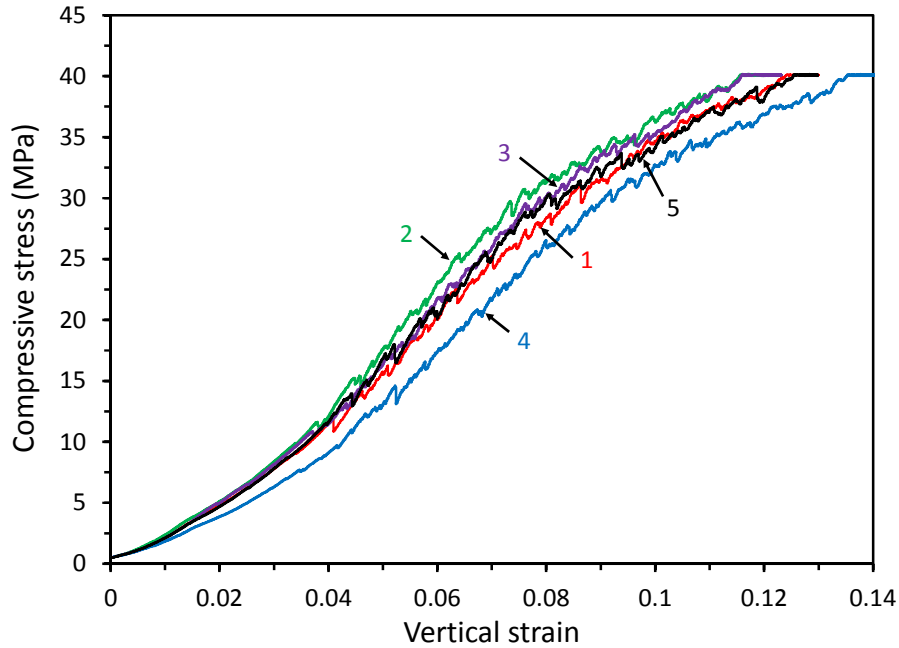


Fig 7. Stress-strain response from five crush tests on G500 sand

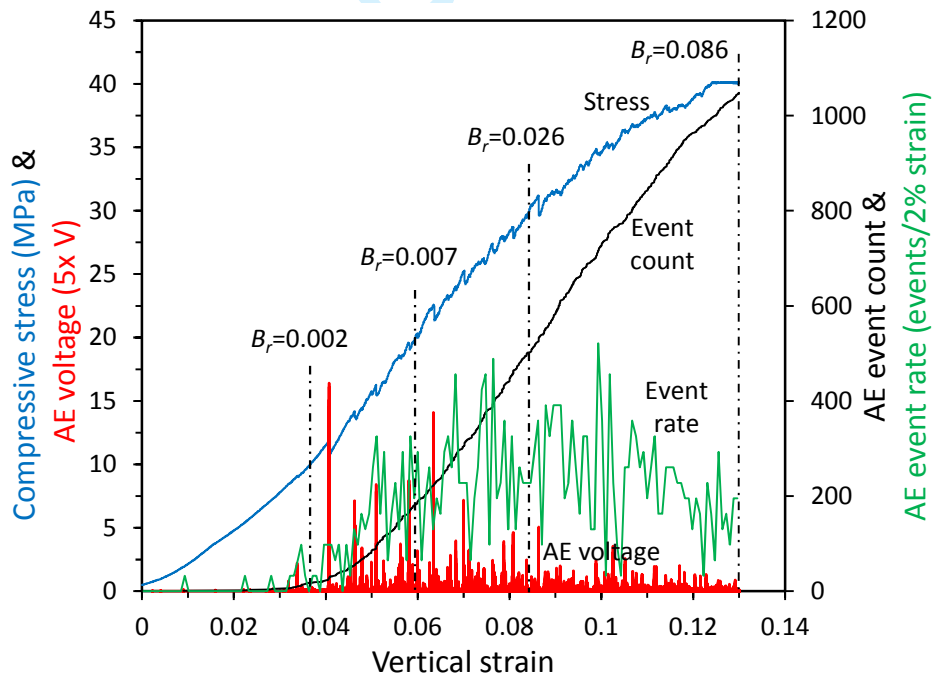


Fig 8. Compressive stress and AE data versus strain for G500 sand (Test 1)

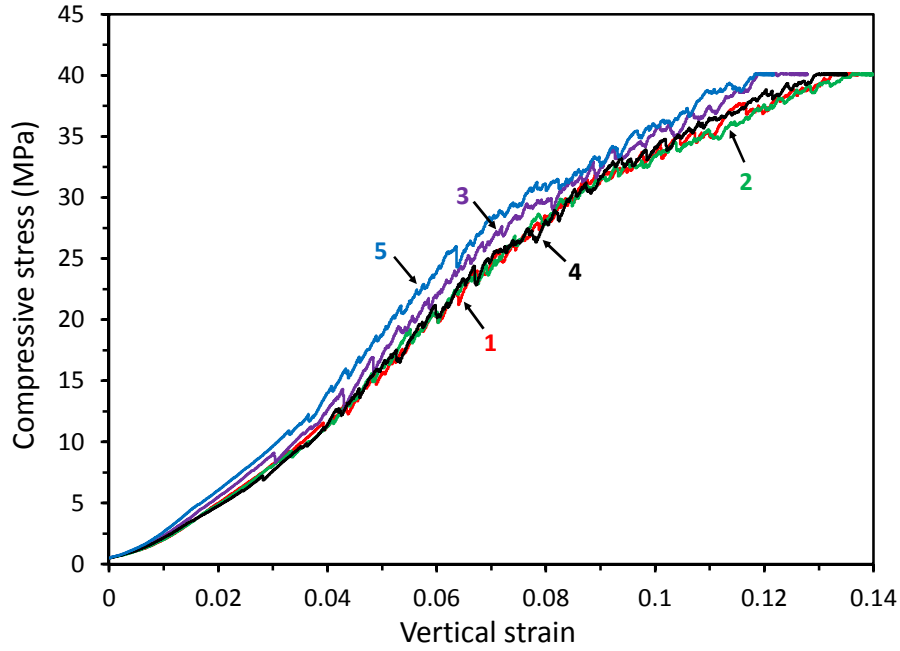


Fig 9. Stress-strain response from five crush tests on G600 sand

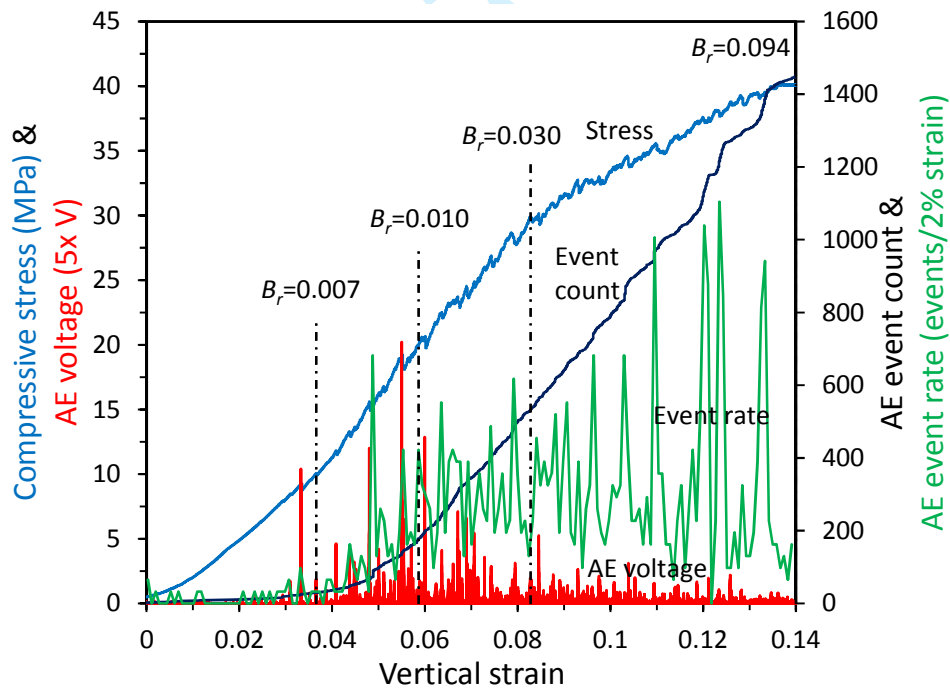


Fig 10. Compressive stress and AE data versus strain for G600 sand (Test 2)

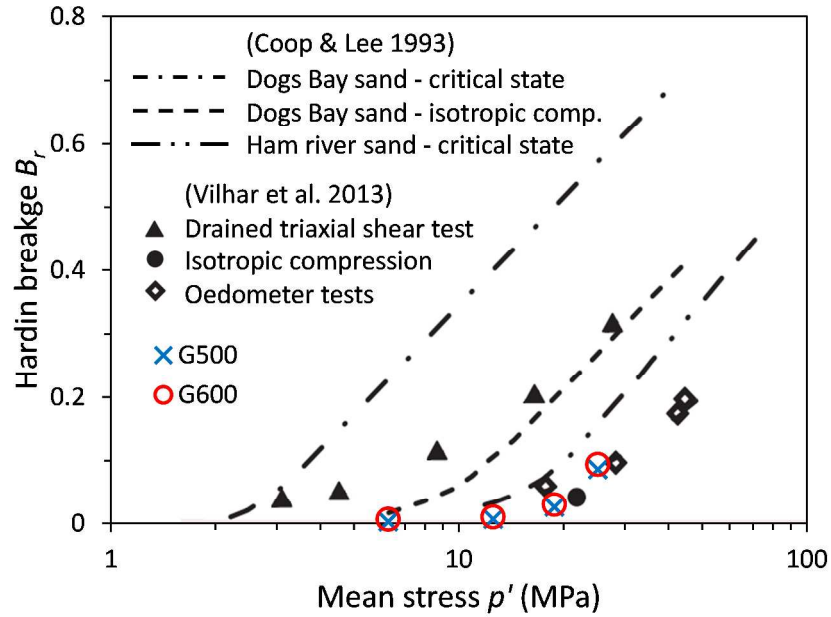


Fig 11. Comparison between particle breakage measured in this study and other test results

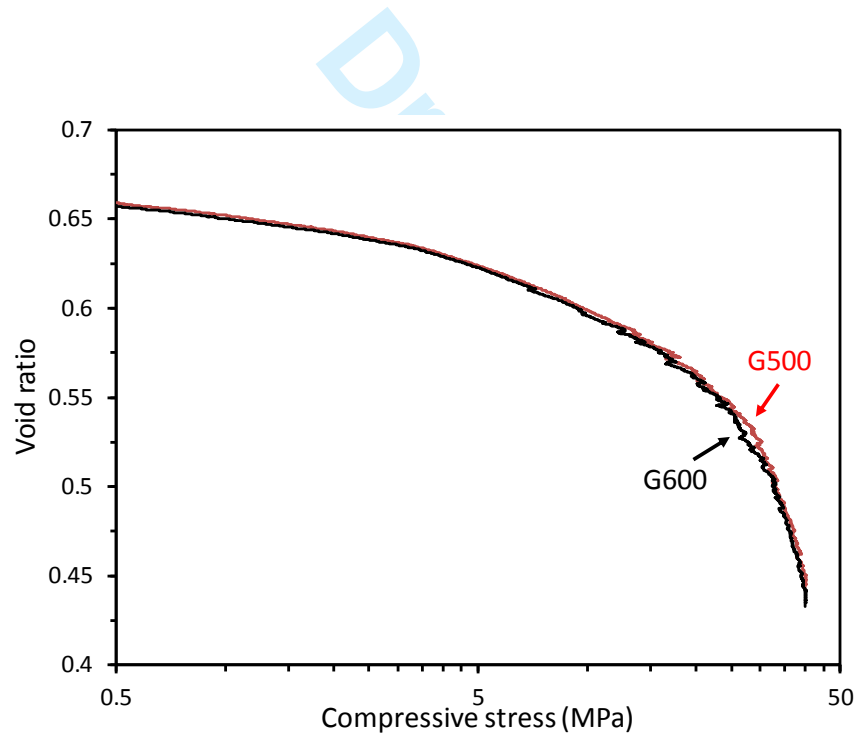


Fig 12. Sand pack void ratio versus compressive stress.

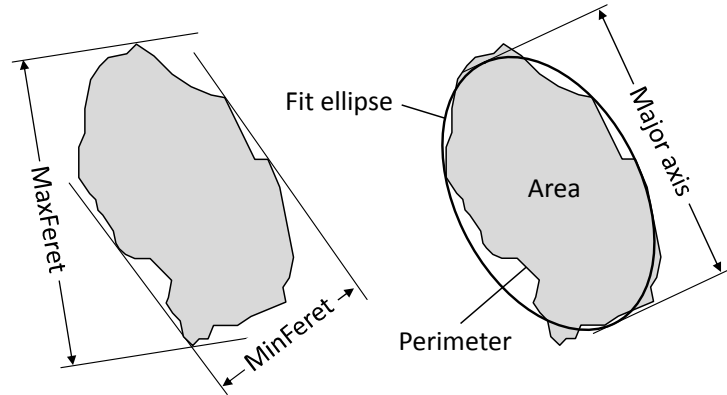


Fig 13. Morphological properties of particle shape

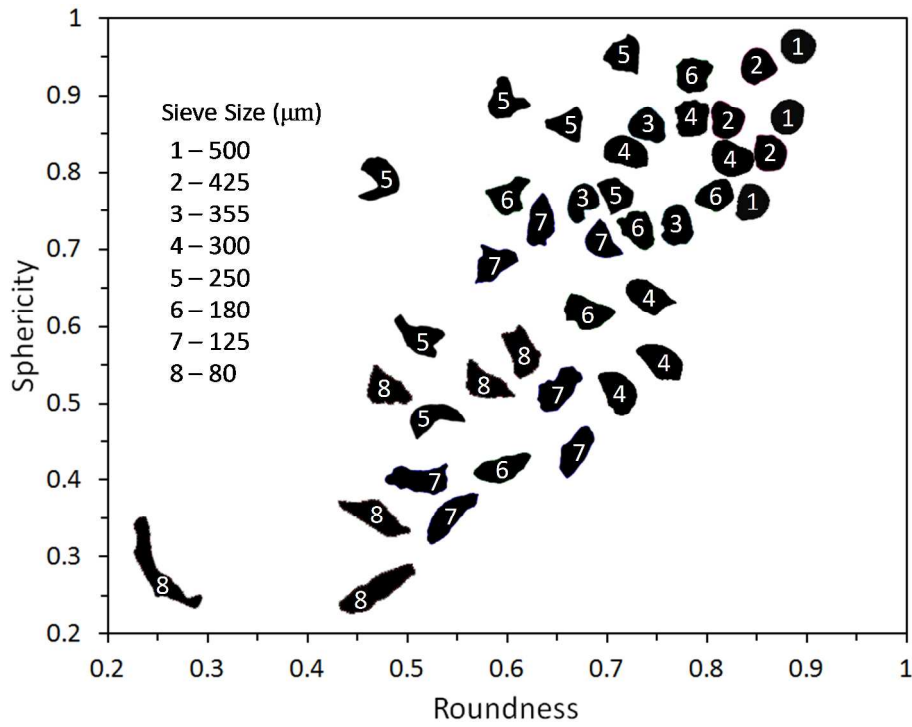


Fig 14. Shape of sand particles (0.08-0.5 mm) along with their measured roundness and sphericity (each particle outline has been scaled to approximately the same size).

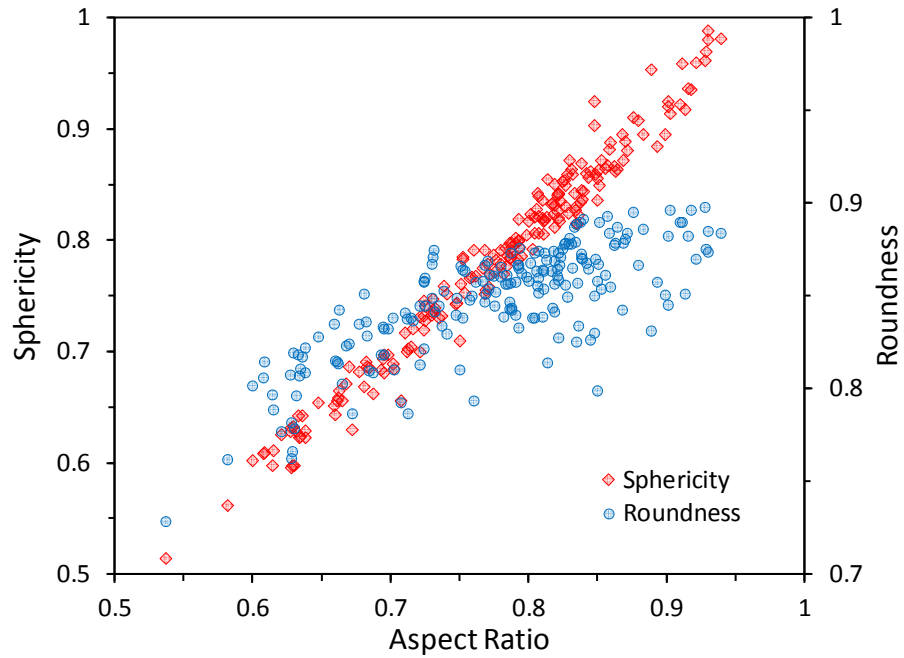


Fig 15. Correlation of sphericity and roundness with aspect ratio for G500 sand

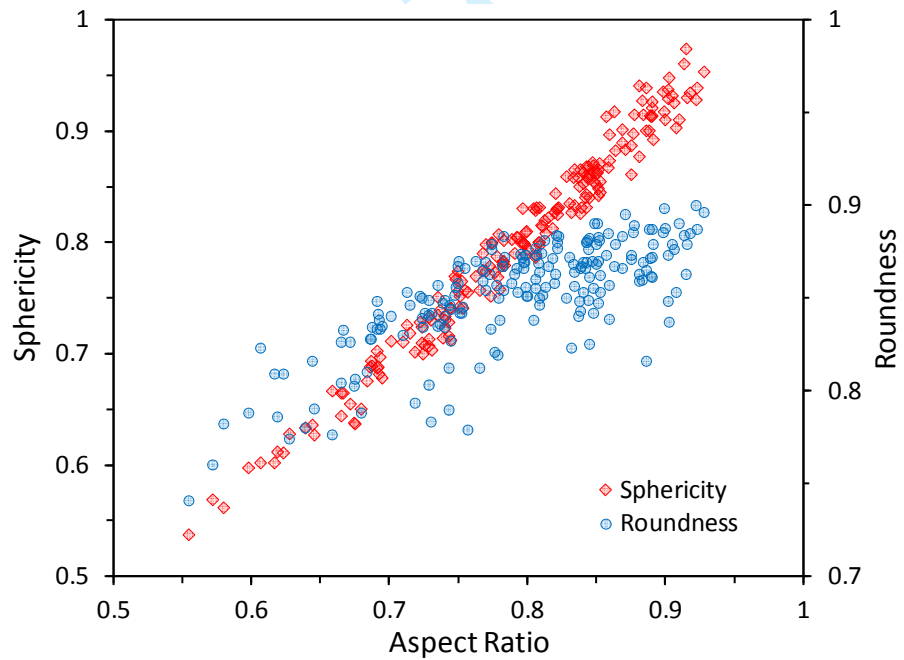


Fig 16. Correlation of sphericity and roundness with aspect ratio for G600 sand

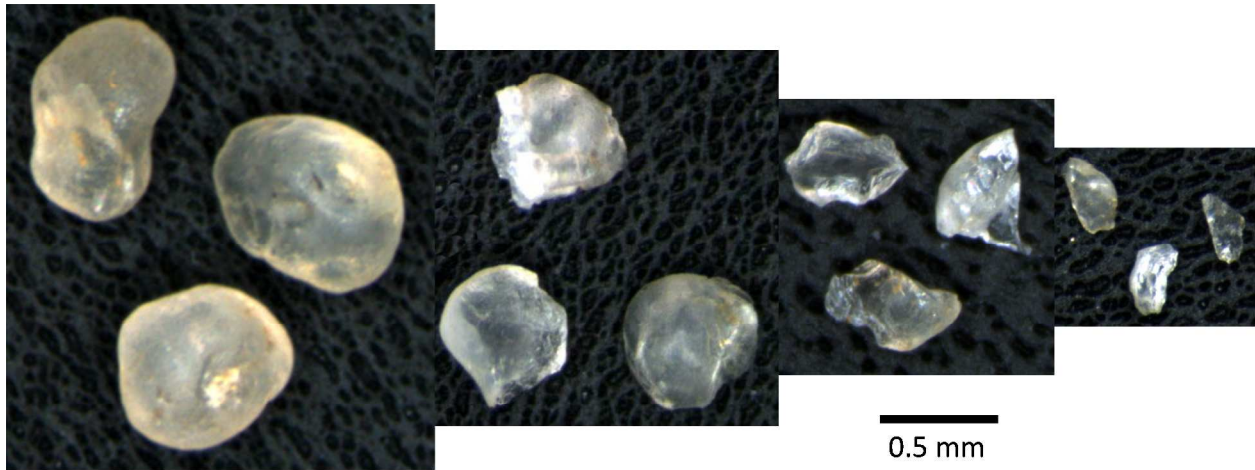


Fig 17. Shape of grains from different sieves (left to right: 0.5, 0.355, 0.25, and 0.125 mm) after a crushing test on G500 sand.

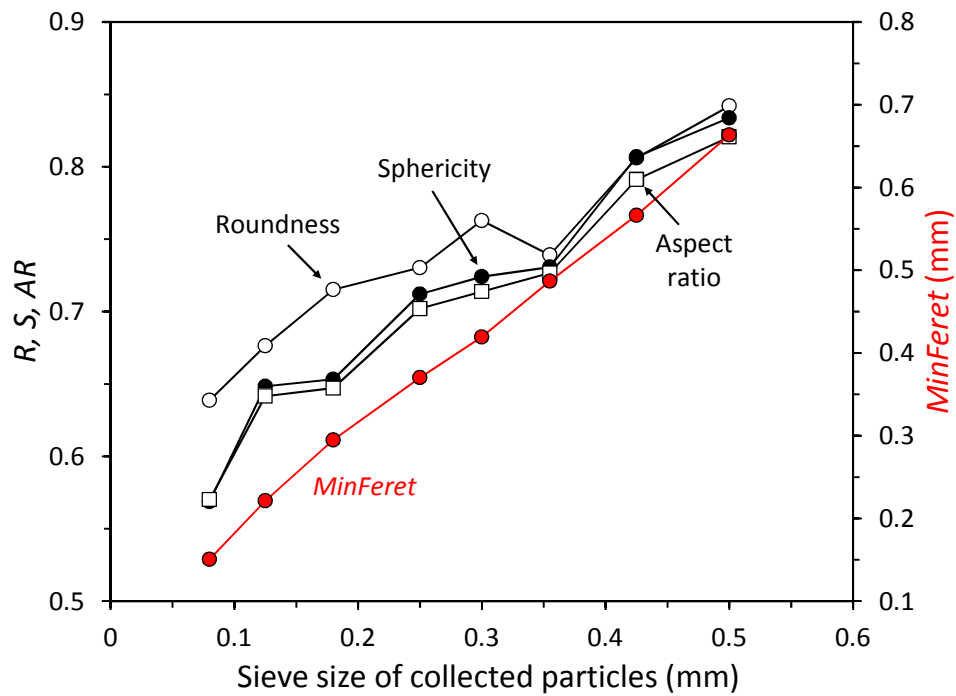


Fig 18. Mean values of geometry descriptors versus sieve size for G500 sand.

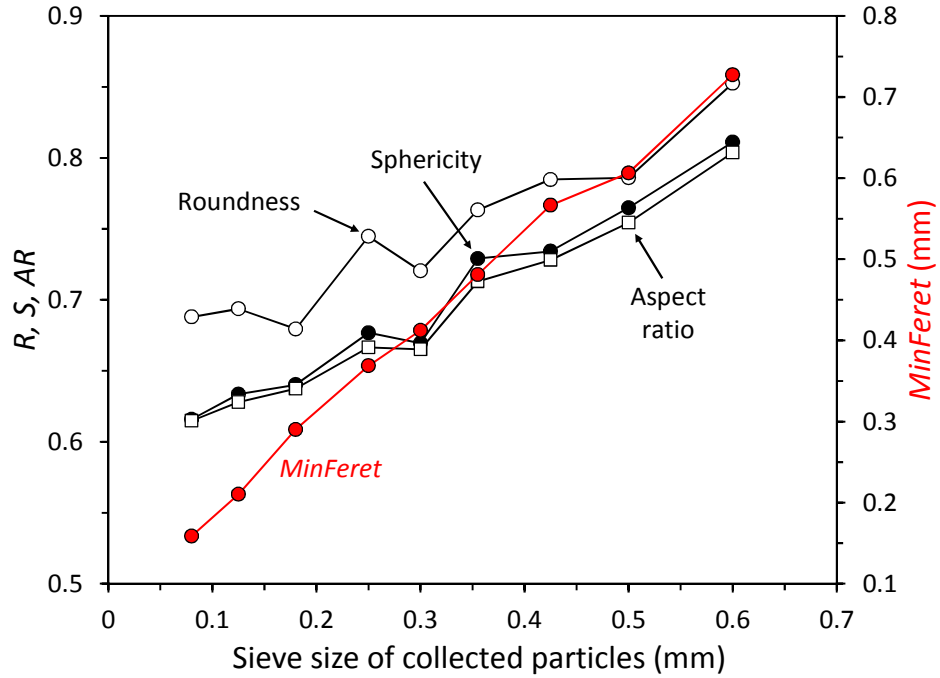


Fig 19. Mean values of geometry descriptors versus sieve size for G600 sand.

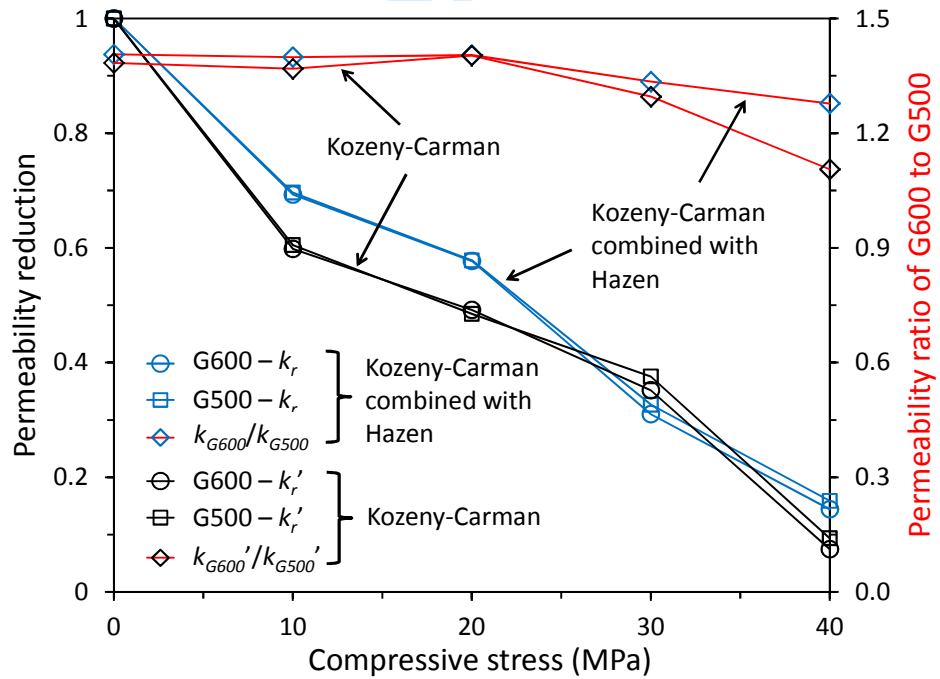


Fig 20. Permeability reduction and permeability ratio of G600 and G500 under different stress